

HVQ-CGIC: Enabling Hyperprior Entropy Modeling for VQ-Based Controllable Generative Image Compression*

Niu Yi
Xidian University
niuyi@mail.xidian.edu.cn

Ma Mingming
Xidian University
mamingming@xidian.edu.cn

Xu Tianyi
Xidian University
25171111417@stu.xidian.edu.cn

Wang Xinkun
Xidian University
25171213993@stu.xidian.edu.cn

December 9, 2025

Abstract

Generative learned image compression methods using Vector Quantization (VQ) have recently shown impressive potential in balancing distortion and perceptual quality. However, these methods typically estimate the entropy of VQ indices using a static, global probability distribution, which fails to adapt to the specific content of each image. This non-adaptive approach leads to untapped bitrate potential and challenges in achieving flexible rate control. To address this challenge, we introduce a **Controllable Generative Image Compression** framework based on a **VQ Hyperprior**, termed HVQ-CGIC. HVQ-CGIC rigorously derives the mathematical foundation for introducing a hyperprior to the VQ indices entropy model. Based on this foundation, through novel loss design, to our knowledge, this framework is the first to introduce RD balance and control into vector quantization-based Generative Image Compression. Cooperating with a lightweight hyper-prior estimation network HVQ-CGIC achieves a significant advantage in rate-distortion (RD) performance compared to current state-of-the-art (SOTA) generative compression methods. On the Kodak dataset, we achieve the same LPIPS as Control-GIC, CDC and HiFiC with an average of 61.3% fewer bits. We posit that HVQ-CGIC has the potential to become a foundational component for VQGAN-based image compression, analogous to the integral role of the Hyper-Prior framework in neural image compression.

1 Introduction

In recent years, deep learning-based image compression has made significant progress [4]. End-to-end optimized autoencoders, enhanced by powerful entropy models such as scale hyperpriors [5] and joint autoregressive priors [37], have become the dominant paradigm. These methods, typically based on Scalar Quantization (SQ), have surpassed classical codecs like VVC [9] on pixel-level fidelity metrics such as PSNR. However, optimizing for pixel-level metrics often leads to perceptually poor results, particularly at low bitrates.

To address this limitation, the research community has shifted focus towards Generative Image Compression (GIC). By incorporating generative models such as Generative Adversarial Networks (GANs) [36] or VQ-VAEs [15], these methods optimize the Rate-Distortion-Perception (RDP) trade-off. This allows them to generate images with high realism and rich textures, even at extremely low bitrates. Among these generative methods, paradigms based on Vector Quantization (VQ) have garnered significant attention for their ability to discretize image features into semantically rich codebook indices (VQ-indices).

Despite VQ’s excellent performance in perceptual reconstruction, it faces a fundamental challenge in efficient entropy modeling and rate control. Most existing VQ-based compression methods assume a static, often uniform, probability distribution for the VQ indices. This assumption completely ignores the strong spatial correlations inherent in natural images. This failure to model content-specific context leads to untapped bitrate potential. Crucially, prior VQ-based codecs lack a learned, content-adaptive probability model for the indices themselves, so the index-rate

*Preprint. Under Review

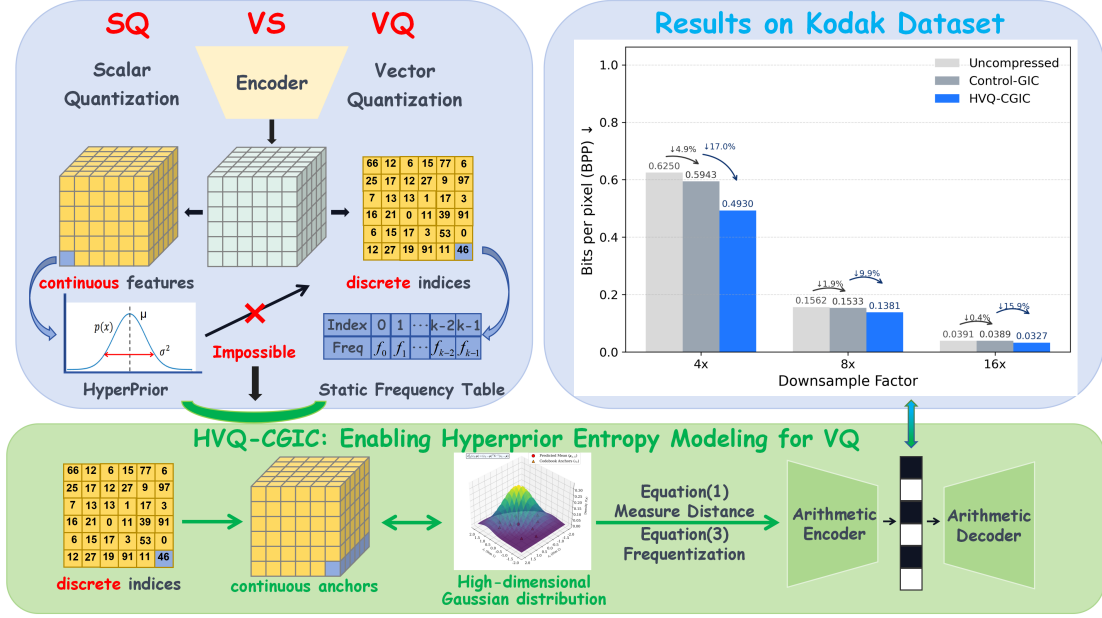


Figure 1: Our HVQ-CGIC breaks through the limitation that VQ cannot design hyperprior entropy models, and achieves significantly lower bitrates than [30] on Kodak under the same downsampling factor.

term is unavailable or constant during training. As a result, the bitrate is steered by manual knobs (codebook size, downsampling) rather than a differentiable rate term. In contrast, our hyperprior provides a learned $P(y|z)$ over the VQ indices and hands RD scheduling over to the network.

The difficulty in solving this problem arises from a fundamental conflict. The most successful entropy models, namely hyperpriors [5], were designed for continuous latent variables in SQ, where they effectively model spatial correlations. However, VQ indices are unordered, discrete symbols. This discrete and unordered nature makes it non-trivial to directly apply a continuous probabilistic model (like a Gaussian) to predict the distribution of VQ indices.

In this paper, we propose **HVQ-CGIC**. Instead of predicting the probability of a discrete index k directly, a hyperprior network predicts at each spatial location the parameters (μ, Σ) of a multivariate Gaussian over the continuous embedding space. Treating the codebook entries $\{e_k\}$ as fixed “anchors”, we convert this continuous density into categorical index probabilities via a Mahalanobis-distance Softmax. For practical (de)coding speed and stability, we then adopt an efficiency-driven simplification and assume an isotropic covariance, $\Sigma = \sigma^2 I$, which reduces the Mahalanobis distance to a scaled squared Euclidean distance and enables highly parallel inference. The resulting formulation yields a learned, content-adaptive categorical distribution $P(y|z)$ over

VQ indices that we train by minimizing cross-entropy, effectively shifting RD scheduling from hand-tuned heuristics to the network. Experimental results demonstrate that HVQ-CGIC achieves state-of-the-art (SOTA) generative compression performance.

Our main contributions are summarized as follows:

- We are the first to propose and mathematically derive a hyperprior entropy model for discrete VQ indices, resolving the conflict between continuous hyperpriors and discrete indices.
- Building on this derivation (§3.2), we design a unified Rate-Distortion (RD) objective that directly minimizes the cross-entropy of the learned $P(y|z)$ and exposes explicit weights on the VQ-index rate and hyper rate, thereby handing RD control to the network.
- We design a new hyperprior-controllable image compression scheme that achieves higher fidelity and realism in image compression under variable bit rates, while keeping the time complexity at the millisecond level with lightweight networks.
- HVQ-CGIC obtains over 61% bit reduction on Kodak with the same LPIPS as the previous SOTA, while demonstrating comprehensive state-of-the-art performance across key rate-distortion-perception metrics.

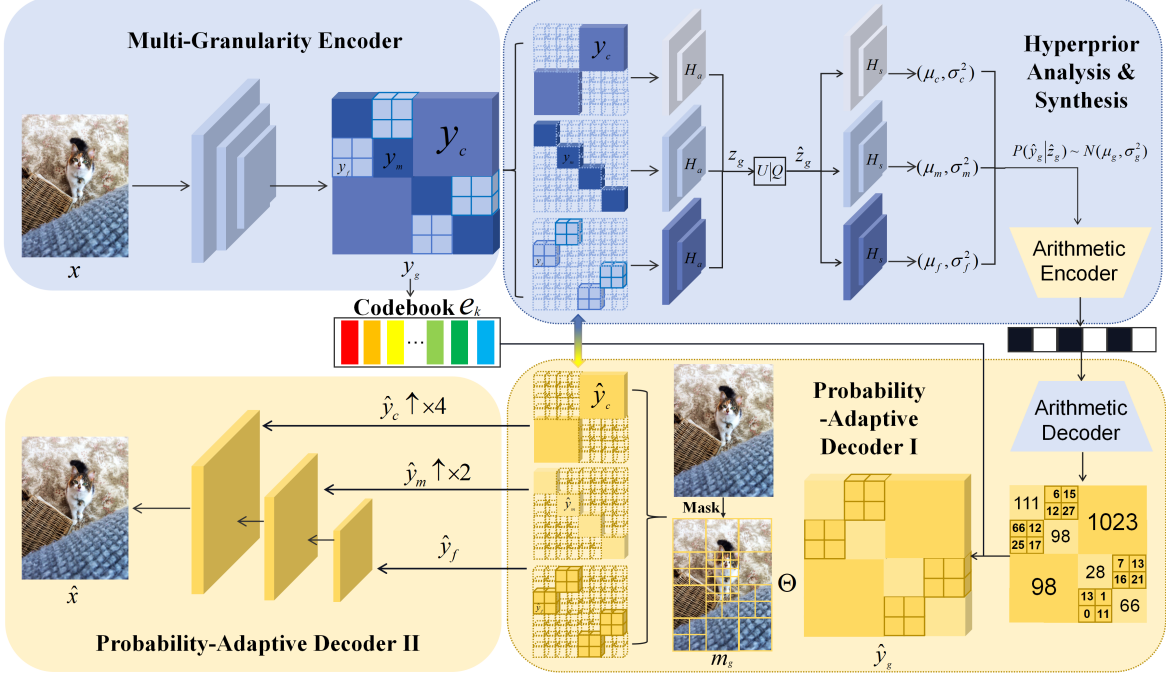


Figure 2: HVQ-CGIC flowchart, details see 3.3. Θ : represents element-wise multiplication here.

2 Related Works and Discussions

2.1 Learned Image Compression

The foundations of lossy image compression are grounded in Shannon’s rate-distortion theory [42]. The seminal work of Ballé et al. [4] established the now-dominant paradigm of end-to-end optimization based on Scalar Quantization (SQ). Subsequent research has rapidly advanced this paradigm on two main fronts: exploring more powerful network architectures and designing more accurate probability models.

On the architecture side, advancements include more sophisticated nonlinear transforms [41, 3, 24, 32], content-adaptive mechanisms [43, 40, 31], and the recent adoption of Transformer [54, 34] and Diffusion-based models [47, 10].

On the entropy modeling side, a major breakthrough was the Hyperprior [5], which uses side information \mathbf{z} to parameterize a conditional probability distribution $p(\hat{\mathbf{y}}|\mathbf{z})$. This, combined with autoregressive priors [35, 37, 27], enabled learned methods to finally outperform traditional codecs like BPG in PSNR. A wide variety of other works have also contributed to R-D performance [12, 11, 33, 38, 36, 49,

19, 46, 17, 25, 50, 18, 23, 45].

While effective, these foundational works are almost exclusively designed for SQ. In contrast, Vector Quantization (VQ), which offers better theoretical rate-distortion properties, has been less common. Early work explored soft-to-hard VQ [1], while a promising recent direction is Lattice Vector Quantization (LVQ), which maintains high efficiency and has been adapted for learned frameworks [51, 16, 29, 52]. However, effectively modeling the entropy of these discrete VQ indices remains a significant challenge.

2.2 Discussion of VQ-based Methods

Several recent works have attempted to address the challenges of VQ-based compression. Zhu et al. [53] proposed a probabilistic vector quantization to estimate means and covariances. However, their optimization goal only considers the distortion term, overlooking the crucial bitrate component. Li et al. [30] (Control-GIC) achieves single-model rate adaptation by dynamically allocating tokens at multiple granularities. This preprocessing-based allocation creates a new paradigm for VQ rate control and served as an inspiration for our work. However, it does not fundamentally solve the problem of precise

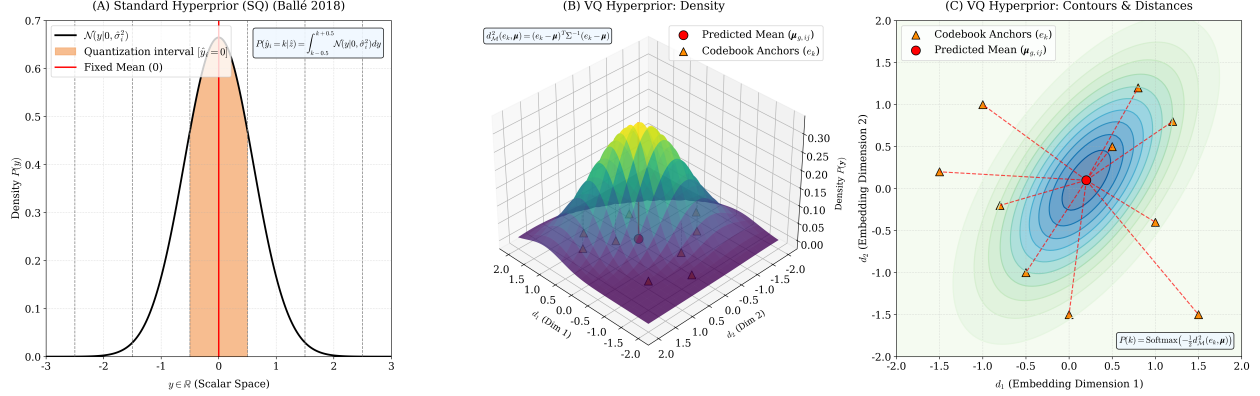


Figure 3: Scalar quantization hyperprior model (a) and our proposed vector quantization hyperprior models (b)(c). Detailed introduction is in §3.2.3.

RD-balance regulation. Jia et al. [22] (GLC) uses a VQ-VAE as a "frontend" to map an image to a continuous latent space, which is then compressed by a standard SQ-Hyperprior pipeline. This hybrid approach is essentially still reliant on scalar quantization for entropy coding, not the VQ indices themselves.

In this paper, we address this specific gap by exploring hyperprior modeling directly within the discrete VQ-based generative compression domain. We design a novel hyperprior paradigm, HVQ-CGIC, which, to our knowledge, is the first to enable true end-to-end RD optimization for the VQ indices, demonstrating superior effectiveness and compression efficiency.

3 Method

3.1 Framework Overview

In this section, we detail the proposed **HVQ-CGIC** framework. To achieve controllable, generative image compression guided by a high-dimensional hyperprior, our model comprises three key components: 1) Multi-Granularity Encoder to map the input image into discrete indices at multiple granularities; 2) Lightweight Hyperprior System to generate content-adaptive probabilities for these indices; and 3) Probability-Adaptive Decoder to reconstruct the final image from the decoded indices.

In the following sections, we first present the **mathematical principle** underlying our VQ hyperprior framework (§3.2), then describe the **network architecture** (§3.3). Finally, the entire framework is trained end-to-end to minimize a unified rate-

distortion objective, which balances distortion D and bitrate consumption R (detailed in §3.4).

3.2 Principle of Hyperprior for VQ Indices

3.2.1 Problem Setting: Bridging Continuous Priors and Discrete Indices

The success of hyperpriors in Scalar Quantization (SQ) [5, 37] arises from predicting Gaussian parameters (μ, σ) for a continuous latent variable, enabling highly efficient entropy coding. However, directly migrating this concept to Vector Quantization (VQ) encounters a **fundamental challenge**. Consider an input image $x \in \mathbb{R}^{3 \times H \times W}$, the encoder outputs a continuous feature map $h_g \in \mathbb{R}^{D \times H_g \times W_g}$. The VQ step maps the D -dimensional feature vector $(h_g)_{ij}$ at each spatial location (i, j) to a discrete index $(\hat{y}_g)_{ij} \in \{1, \dots, K\}$. These indices are **discrete and unordered** symbols, lacking the **continuous spatial structure** inherent in SQ latents upon which SQ hyperpriors rely. Therefore, constructing a probability model $P(\hat{y}_g | \hat{z}_g)$ for VQ indices at each granularity g that is similarly **content-adaptive** and **spatially varying** to enable efficient entropy coding is a critical challenge.

3.2.2 Core Idea: Gaussian Prior in the Embedding Space

Our **key insight** is that while the indices $(\hat{y}_g)_{ij}$ are discrete, their corresponding codebook embedding vectors $\mathbf{e}_k \in \mathbb{R}^D$ reside in a **continuous D-dimensional embedding space**. Therefore, we propose **not to model the index k directly**,

but instead predict a conditional probability distribution within this continuous embedding space. Specifically, for each granularity $g \in \{c, m, f\}$, an independent hyperprior branch processes the corresponding feature y_g through a HyperAnalysis network to generate a **continuous** hyper-latent variable z_g . **To simulate quantization effects and for transmission, z_g is quantized into \hat{z}_g :** during training, we add uniform noise $z_g + \mathcal{U}(-0.5, 0.5)$; during inference, we use rounding $\hat{z}_g = \text{round}(z_g)$. Subsequently, the HyperSynthesis network utilizes \hat{z}_g to predict, at each spatial location (i, j) of the granularity- g indices, the **parameters of a multivariate Gaussian distribution**, $\Theta_{g,ij}(\hat{z}_g) = (\boldsymbol{\mu}_{g,ij}, \boldsymbol{\Sigma}_{g,ij})$. Here, the mean $\boldsymbol{\mu}_{g,ij} \in \mathbb{R}^D$ represents the **expected feature vector** (in the embedding space) at that location, and the covariance matrix $\boldsymbol{\Sigma}_{g,ij} \in \mathbb{R}^{D \times D}$ captures the uncertainty.

3.2.3 From Continuous Gaussian to Discrete Probabilities via Mahalanobis Distance

The next step is to **bridge the continuous Gaussian parameters $(\boldsymbol{\mu}_{g,ij}, \boldsymbol{\Sigma}_{g,ij})$ to the probabilities $P((\hat{y}_g)_{ij} = k | \hat{z}_g)$ of the discrete indices k** . We treat the codebook embeddings \mathbf{e}_k as fixed "anchors" in the embedding space. We hypothesize that the probability of selecting index k at location (i, j) is related to the "distance" of its anchor \mathbf{e}_k from the predicted Gaussian distribution $\mathcal{N}(\boldsymbol{\mu}_{g,ij}, \boldsymbol{\Sigma}_{g,ij})$. We use the squared **Mahalanobis Distance** to measure this distance, as it accounts for the covariance $\boldsymbol{\Sigma}_{g,ij}$:

$$d_{\mathcal{M}}^2(\mathbf{e}_k, \boldsymbol{\mu}_{g,ij}) = (\mathbf{e}_k - \boldsymbol{\mu}_{g,ij})^\top (\boldsymbol{\Sigma}_{g,ij})^{-1} (\mathbf{e}_k - \boldsymbol{\mu}_{g,ij}) \quad (1)$$

We normalize the negative exponential of this distance using the Softmax function to obtain the final categorical probability distribution:

$$P((\hat{y}_g)_{ij} = k | \hat{z}_g) = \frac{\exp(-\frac{1}{2}d_{\mathcal{M}}^2(\mathbf{e}_k, \boldsymbol{\mu}_{g,ij}))}{\sum_{\ell=1}^K \exp(-\frac{1}{2}d_{\mathcal{M}}^2(\mathbf{e}_\ell, \boldsymbol{\mu}_{g,ij}))} \quad (2)$$

This provides information-theoretic justification for our model (details see Supplementary Material).

Simplification in Practice (Isotropic Assumption): In our actual implementation, for computational efficiency and stability, we assume the covariance matrix is diagonal and isotropic, i.e., $\boldsymbol{\Sigma}_{g,ij} = (\sigma_{g,ij})^2 \mathbf{I}$, where $\sigma_{g,ij} \in \mathbb{R}^+$ is a scalar standard deviation. Under this simplification, the Mahalanobis distance reduces to the squared **Euclidean distance** divided by the variance:

$$P((\hat{y}_g)_{ij} = k | \hat{z}_g) = \frac{\exp\left(-\frac{\|\mathbf{e}_k - \boldsymbol{\mu}_{g,ij}\|^2}{2(\sigma_{g,ij})^2}\right)}{\sum_{\ell=1}^K \exp\left(-\frac{\|\mathbf{e}_\ell - \boldsymbol{\mu}_{g,ij}\|^2}{2(\sigma_{g,ij})^2}\right)} \quad (3)$$

Intuition: As illustrated in Fig 3, while SQ hyperpriors predict a Gaussian on 1D line, our method predicts a Gaussian probability "cloud" in the D-dimensional (visualized as $D = 2$) embedding space. Its center is determined by $\boldsymbol{\mu}_{g,ij}$, and its shape and spread are controlled by $\sigma_{g,ij}$. The codebook vectors \mathbf{e}_k act as anchors in this space; those closer to the cloud's center receive higher probability. The covariance reflects the model's uncertainty about the feature at that location, influencing the concentration of the probability distribution, and thus the bitrate.

3.2.4 Implications for Efficient Entropy Coding

The core value of Equation (3) lies in providing a complete categorical probability distribution $P_{g,ij} = \{p_{g,ij,k}\}_{k=1}^K$ over the VQ index $(\hat{y}_g)_{ij}$ at (i, j) for each granularity g . This distribution $P_{g,ij}$ is **content-adaptive** and **spatially varying**, making it directly suitable for input into standard entropy coders, such as an Arithmetic Coder. And in essence, it is an ultra-high-dimensional context that is superior to any hand-crafted context. According to information theory, arithmetic coding a symbol using the predicted probability distribution $P_{g,ij}$ achieves an expected code length close to its Shannon entropy $H(P_{g,ij}) = -\sum_{k=1}^K p_{g,ij,k} \log_2 p_{g,ij,k}$. The expected bitrate for encoding all VQ indices at granularity g can be expressed as:

$$\begin{aligned} R_{\hat{y}_g} &= \mathbb{E}_x \left[\sum_{i,j} H(P_{g,ij}^*, P_{g,ij}) \right] \\ &= \mathbb{E}_x \left[\sum_{i,j} (H(P_{g,ij}^*) + D_{\text{KL}}(P_{g,ij}^* \parallel P_{g,ij})) \right] \end{aligned} \quad (4)$$

where $P_{g,ij}^*$ denotes the real but unknown distribution of index $(\hat{y}_g)_{ij}$ given image x , and $H(P_{g,ij}^*, P_{g,ij})$ is the cross-entropy. Based on this principle, we directly minimize the cross-entropy to update the Gaussian parameters $(\boldsymbol{\mu}_{g,ij}, \sigma_{g,ij})$ via backpropagation, driving the predicted distribution to match the true posterior. The complete rate-distortion objective is detailed in §3.4.

3.3 Module Design

This section maps the VQ hyperprior principles detailed in §3.2 onto the network modules of HVQ-CGIC, following the overall pipeline illustrated in Fig 2.

3.3.1 Multi-Granularity Encoder and Vector Quantization

Our Multi-Granularity Encoder E distills hierarchical representations from the input image $x \in \mathbb{R}^{3 \times H \times W}$ at three progressively finer granularities:

$$\{y_c, y_m, y_f\} = E(x) \quad (5)$$

where $y_c \in \mathbb{R}^{D \times H/16 \times W/16}$, $y_m \in \mathbb{R}^{D \times H/8 \times W/8}$, and $y_f \in \mathbb{R}^{D \times H/4 \times W/4}$ represent coarse-grained, medium-grained, and fine-grained features, respectively. The Vector Quantization module then maps each continuous feature vector at every spatial location to its nearest entry in a shared codebook $\mathcal{E} = \{\mathbf{e}_k\}_{k=1}^K$, where $\mathbf{e}_k \in \mathbb{R}^D$:

$$(\hat{y}_g)_{ij} = Q_y((y_g)_{ij}) = \arg \min_{k \in \{1, \dots, K\}} \|(y_g)_{ij} - \mathbf{e}_k\|^2 \quad (6)$$

This produces discrete index maps $\hat{y}_g \in \{1, \dots, K\}^{H_g \times W_g}$ for each granularity $g \in \{c, m, f\}$. The use of a single shared codebook across all granularities ensures consistent semantic representation while reducing model complexity.

3.3.2 Independent Hyperprior Branches

For each granularity $g \in \{c, m, f\}$, an independent hyperprior branch consists of HyperAnalysis H_a and HyperSynthesis H_s networks. First, H_a compresses feature y_g into a continuous hyper-latent z_g :

$$z_g = H_a(y_g) \quad (7)$$

During training, z_g is quantized via additive uniform noise: $\hat{z}_g = z_g + \mathcal{U}(-0.5, 0.5)$; during inference, we use rounding: $\hat{z}_g = \text{round}(z_g)$. Subsequently, H_s generates the Gaussian parameters at the spatial resolution corresponding to granularity g :

$$(\boldsymbol{\mu}_g, \sigma_g) = H_s(\hat{z}_g) \quad (8)$$

where $\boldsymbol{\mu}_g \in \mathbb{R}^{D \times H_g \times W_g}$ and $\sigma_g \in \mathbb{R}^{1 \times H_g \times W_g}$. These parameters are used to compute the conditional probabilities $P(\hat{y}_g | \hat{z}_g)$ via Eq. (3).

3.3.3 Entropy Coding and Bitstream

The final bitstream consists of three components for each active granularity g : (1) **VQ Indices** \hat{y}_g , arithmetically coded using probabilities $P(\hat{y}_g | \hat{z}_g)$ and masked by routing mask $m_g \in \{0, 1\}^{H_g \times W_g}$, which is manually allocated based on pre-defined strategies to determine active spatial regions at each granularity. (2) **Hyper-latent** \hat{z}_g , where only the subset corresponding to active spatial regions (determined by m_g) is encoded. (3) **Routing**

Masks $\{m_c, m_m, m_f\}$, losslessly compressed to indicate which granularity is used at each location. We will further discuss the strategy of Routing Mask in the supplementary materials.

3.3.4 Probability-Adaptive Decoder

The decoder D receives the decoded indices $\{\hat{y}_c, \hat{y}_m, \hat{y}_f\}$ and masks $\{m_c, m_m, m_f\}$. For each granularity g , the indices $\hat{y}_g \in \{1, \dots, K\}^{H_g \times W_g}$ are mapped back to their corresponding codebook embeddings via lookup: at each spatial location (i, j) in the granularity- g grid, the discrete index $(\hat{y}_g)_{ij}$ retrieves the embedding vector $\mathbf{e}_{(\hat{y}_g)_{ij}} \in \mathbb{R}^D$ from the codebook \mathcal{E} . These embedding maps from all three granularities are then upsampled to the finest resolution and fused into a unified feature map $\mathbf{e}_{\text{fused}}$. At each location (i, j) on the finest grid:

$$(\mathbf{e}_{\text{fused}})_{ij} = \sum_{g \in \{c, m, f\}} [\text{Lookup}(\hat{y}_g, \mathcal{E}) \uparrow S_g]_{ij} \cdot (m_g \uparrow S_g)_{ij} \quad (9)$$

where $\text{Lookup}(\hat{y}_g, \mathcal{E})$ denotes the codebook lookup operation that produces a feature map of size $\mathbb{R}^{D \times H_g \times W_g}$, S_g is the upsampling factor, and $\uparrow S_g$ denotes spatial upsampling. Finally, the decoder reconstructs the image:

$$\hat{x} = D(\mathbf{e}_{\text{fused}}) \quad (10)$$

3.4 Loss Function and Training Strategy

3.4.1 Unified Rate-Distortion Objective

The entire framework minimizes a unified rate-distortion objective balancing reconstruction quality and bitrate. The total loss \mathcal{L} balances distortion D and bitrate consumption R :

$$\mathcal{L} = \mathbb{E}[D(x, \hat{x})] + \sum_{g \in \{c, m, f\}} (\lambda_{y,g} R_{\hat{y}_g} + \lambda_{z,g} R_{\hat{z}_g}) \quad (11)$$

$$D(x, \hat{x}) = \mathcal{L}_{\text{rec}} + \mathcal{L}_{\text{percep}} + \lambda_{\text{GAN}} \mathcal{L}_{\text{GAN}} + \lambda_{\text{VQ}} \mathcal{L}_{\text{VQ}} \quad (12)$$

where $\mathcal{L}_{\text{rec}} = \|x - \hat{x}\|_2^2$ is the MSE reconstruction loss, $\mathcal{L}_{\text{percep}}$ is the LPIPS perceptual loss, the adversarial loss is:

$$\mathcal{L}_{\text{GAN}} = -\log D(\hat{x}) \quad (13)$$

where D is a PatchGAN discriminator. The VQ commitment loss is:

$$\mathcal{L}_{\text{VQ}} = \sum_{g \in \{c, m, f\}} (\|\text{sg}[y_g] - \mathbf{e}_{\hat{y}_g}\|_2^2 + \beta \|\text{sg}[\mathbf{e}_{\hat{y}_g}] - y_g\|_2^2) \quad (14)$$

where $\text{sg}[\cdot]$ denotes the stop-gradient operator, $\mathbf{e}_{\hat{y}_g}$ represents the quantized features via codebook lookup, and $\beta = 0.25$. The rate term accounts for VQ indices and hyper-latents:

$$R = \sum_{g \in \{c, m, f\}} (\lambda_{y,g} R_{\hat{y}_g} + \lambda_{z,g} R_{\hat{z}_g}) \quad (15)$$

where $R_{\hat{y}_g} = \mathbb{E}_x \left[\sum_{i,j} H(P_{g,ij}^*, P_{g,ij}) \right]$ is the cross-entropy for VQ indices (derived in §3.2), and $R_{\hat{z}_g}$ is the hyper-latent bitrate via factorized entropy model. Routing masks are losslessly compressed and omitted from R .

3.4.2 Progressive Training Strategy

To ensure stable convergence, we adopt a three-stage progressive training strategy:

Stage A (VQGAN Training): We first train a high-quality VQGAN [15] consisting of encoder E , decoder D , vector quantizer Q_y , and PatchGAN discriminator. Only the distortion term is optimized:

$$\mathcal{L}_A = D(x, \hat{x}) \quad (16)$$

At this stage, the hyperprior networks $\{H_a, H_s\}$ are not yet introduced. This stage establishes a strong perceptually-aligned reconstruction baseline through adversarial training.

Stage B (Hyperprior Training): We load the pre-trained VQGAN weights and freeze all VQGAN parameters. The hyperprior networks $\{H_a, H_s\}$ are initialized and trained exclusively by minimizing the rate term:

$$\mathcal{L}_B = R \quad (17)$$

This forces the hyperprior to learn efficient probability predictions for the fixed VQ indices produced by the frozen VQGAN encoder.

Stage C (Joint Fine-tuning): We fine-tune the entire framework end-to-end with a reduced learning rate:

$$\mathcal{L}_C = D(x, \hat{x}) + R \quad (18)$$

This allows the VQGAN and hyperprior to co-adapt, achieving the optimal rate-distortion-perception trade-off.

4 Experiments

4.1 Experimental Setup

Training details. We train HVQ-CGIC on the OpenImages [26] dataset. We randomly crop images to a uniform resolution of 256×256 . The codebook

$\mathcal{E} \in \mathbb{R}^{k \times d}$ contains $k = 1024$ code vectors, with each code vector having a dimension of $d = 4$. The training is conducted on 4 NVIDIA RTX 4090 GPUs, with a learning rate of 5×10^{-5} and batch size of 2 for 300,000 iterations in Stage A; a learning rate of 2×10^{-5} and batch size of 4 for 150,000 iterations in Stage B; and in Stage C, the learning rate gradually decreases from 1×10^{-5} to 5×10^{-6} with batch size of 2 for 150,000 iterations. Throughout the training process, Stage A maintains a ratio of (0.1, 0.3, 0.6) for coarse, medium, and fine granularities, while Stages B and C use a ratio configuration of (0.3, 0.3, 0.4). During the inference stage, images of arbitrary resolutions can be compressed according to any ratio to achieve rate control.

Evaluation dataset & metrics. We evaluate HVQ-CGIC on Kodak[13] dataset. We also show the results on DIV2K[2], CLIC 2020[44] test set and more details in supplementary material. We measure bitstream size through bits per pixel (bpp). Our evaluation metrics are comprehensive, including perceptual metrics LPIPS[48] and DISTS[14], no-reference perceptual metrics FID[20], NIQE[39] and KID[8], IS[6], and pixel-level distortion metrics PSNR. We provide multi-dimensional comparisons in the experimental section to demonstrate the effectiveness of our method.

Baseline methods. We evaluate our method against recent state-of-the-art (SOTA) neural image compression (NIC) methods. In terms of generative compression methods: 1) HiFiC(NIPS’20)[36] is an influential method using conditional GANs. 2) CDC(NIPS’24)[47] is a representative diffusion-based lossy compression method. Additionally, we compare with SOTA variable-rate and progressive methods: 3) SCR(NIPS’22)[28] proposes a 3D importance map adjusted by quality levels to determine the selected representation elements, thus achieving variable-rate NIC. 4) CTC(CVPR’23)[21] features a bitstream that can be truncated at any point via progressive decoding to finely adjust bitrates. 5) ControlGIC(ICLR’25)[30] has a relatively good traditional entropy coding strategy, so we use it as a complete benchmark for bpp comparison and RD baseline. 6) We use two traditional codecs BPG[7] and VVC[9] for comparison, as well as 7) M&S(Hyperprior)[5] as a reference for classical NIC methods.

4.2 Main Results

Figure 4 demonstrates that HVQ-CGIC shows significant improvements in performance across four metrics: LPIPS, NIQE, DISTS, IS and FID achieving new SOTA results. We provide additional compari-

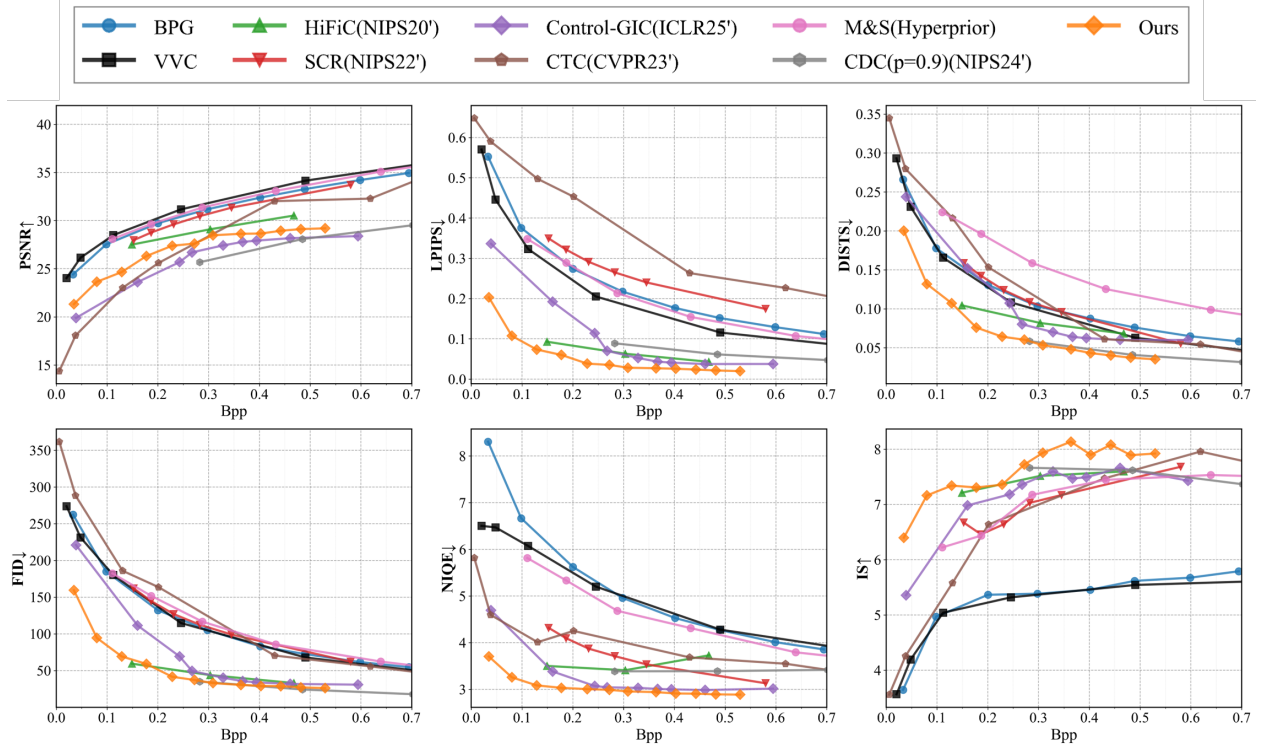


Figure 4: Comparison of Methods on Kodak Dataset.

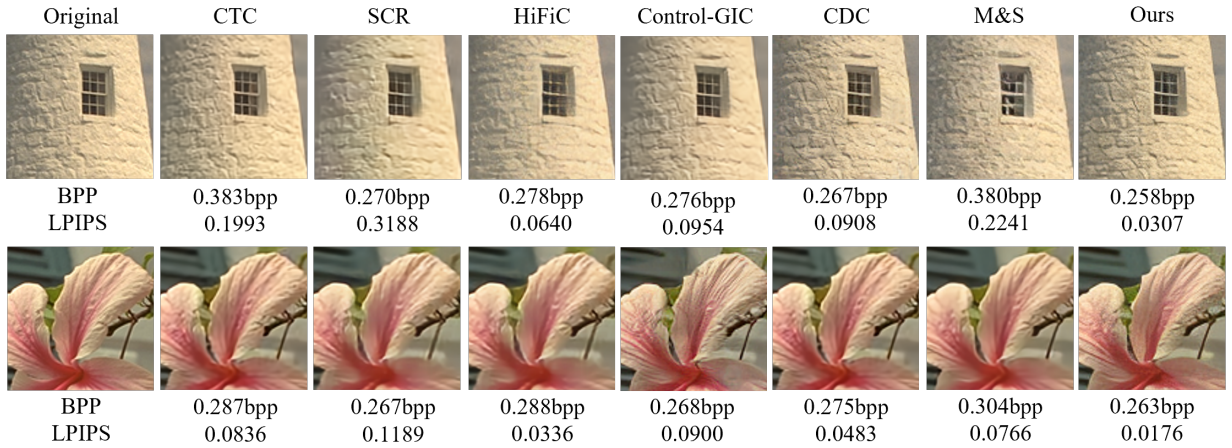


Figure 5: Conduct quantitative comparisons with the listed Baseline Methods.

Method	BPP(\downarrow)	LPIPS(\downarrow)	Enc.(ms)	Dec. (ms)
No Compression	0.625	-	-	-
Control-GIC[30]	0.594(-4.9%)	0.0248	8.43	18.1
1st-Order	0.587(-6.0%)	0.0248	4.66	9.04
2nd-Order	0.584(-6.6%)	0.0248	32.9	48.4
3rd-Order	0.583(-6.7%)	0.0248	145.2	190.2
HVQ-CGIC(RD)	0.530(-15.2%)	0.0197	2.78	4.98
HVQ-CGIC(BPP)	0.493(-21.1%)	0.0278	2.71	4.17

Table 1: Ablation study on the Kodak dataset (downsampling factor 4). Percentages in green indicate relative improvements over the No Compression baseline. The **Enc.** and **Dec.** is the sum of the hyperprior network inference time and arithmetic coding time.

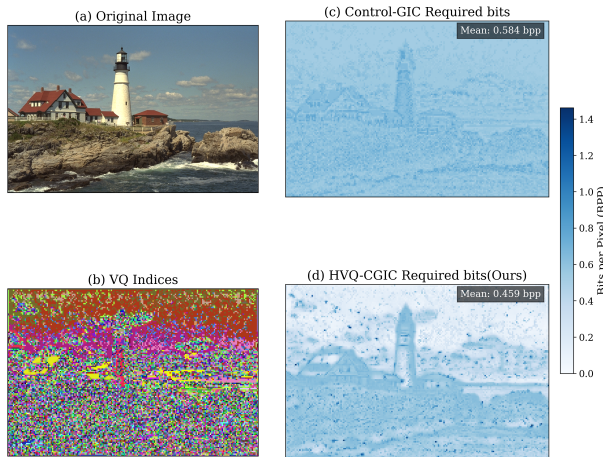


Figure 6: Comparison of Methods on *Kodim21*.

son results for high-resolution images on DIV2K and CLIC2020 in the Supplementary Material.

4.3 Ultimate Entropy Coding Performance

To demonstrate where the limits of hyperpriors lie, we increased the weights of $\lambda_{y,g}$ and $\lambda_{z,g}$ from 1.5×10^{-3} to 1.5×10^{-2} on the RD-balanced model (the HVQ-CGIC(RD) model used for testing in 4.2), while fixing λ_{GAN} at 0.1 and λ_{VQ} at 1, although this would lead to a decline in image reconstruction quality.

We improved the statistical entropy coding strategy used by Control-GIC to adaptive arithmetic entropy coding strategies with multiple high-order context designs (as shown in Figure 7), which do not

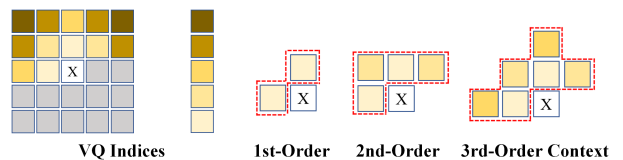


Figure 7: In addition to the context designs shown in the above figure, these three entropy coding strategies also perform adaptive arithmetic coding by updating encoding frequencies in real-time based on the data used for testing, building upon statistical entropy coding.

change the image reconstruction quality. Table 1 provides a comparison of these methods with HVQ-CGIC. It can be seen that the index-based context design in traditional entropy coding shows obvious diminishing marginal effects when the order becomes higher, and more context computation overhead does not bring better context improvement. This proves that HVQ-CGIC actually implements ultra-high-order context encoding through an extremely lightweight network, mining the correlations between features in the latent space.

To better help everyone understand HVQ-CGIC, we also visualized the bit usage distribution of *Kodim21* at $x4$ downsampling ratio compared to Control-GIC in Fig 6. As shown in the figure, HVQ-CGIC almost exhausts every bit of coding redundancy in the latent feature space under similar image textures, saving over 21.4% compared to Control-GIC on the single image.

We also conducted a more **comprehensive comparison** of HVQ-CGIC and other Baseline methods

in terms of **network parameters**, **encoding and decoding time**, and **RD**. Due to space limitations, we present the results in the supplementary material.

5 Conclusion

In this paper, we presented HVQ-CGIC, the first framework to rigorously introduce a hyperprior entropy model for VQ-based compression, thereby enabling true Rate-Distortion (RD) optimization for VQ indices. We believe this work provides a foundational component for VQGAN-based compression and will inspire further exploration into precise RD-Perception control for future generative codecs.

References

- [1] Eirikur Agustsson, Fabian Mentzer, Michael Tschannen, Lukas Cavigelli, Radu Timofte, Luca Benini, and Luc V Gool. Soft-to-hard vector quantization for end-to-end learning compressible representations. *Advances in neural information processing systems*, 30, 2017.
- [2] Eirikur Agustsson and Radu Timofte. Ntire 2017 challenge on single image super-resolution: Dataset and study. In *Proceedings of the IEEE conference on computer vision and pattern recognition workshops*, pages 126–135, 2017.
- [3] Eirikur Agustsson, Michael Tschannen, Fabian Mentzer, Radu Timofte, and Luc Van Gool. Generative adversarial networks for extreme learned image compression. In *Proceedings of the IEEE/CVF international conference on computer vision*, pages 221–231, 2019.
- [4] Johannes Ballé, Valero Laparra, and Eero P Simoncelli. End-to-end optimized image compression. *arXiv preprint arXiv:1611.01704*, 2016.
- [5] Johannes Ballé, David Minnen, Saurabh Singh, Sung Jin Hwang, and Nick Johnston. Variational image compression with a scale hyperprior. *arXiv preprint arXiv:1802.01436*, 2018.
- [6] Shane Barratt and Rishi Sharma. A note on the inception score. *arXiv preprint arXiv:1801.01973*, 2018.
- [7] Fabrice Bellard. BPG image format. <https://bellard.org/bpg/>, 2018.
- [8] Mikołaj Bińkowski, Danica J Sutherland, Michael Arbel, and Arthur Gretton. Demystifying mmd gans. *arXiv preprint arXiv:1801.01401*, 2018.
- [9] Benjamin Bross, Ye-Kui Wang, Yan Ye, Shan Liu, Jianle Chen, Gary J Sullivan, and Jens-Rainer Ohm. Overview of the versatile video coding (vvc) standard and its applications. *IEEE Transactions on Circuits and Systems for Video Technology*, 31(10):3736–3764, 2021.
- [10] Marlene Careil, Matthew J Muckley, Jakob Verbeek, and Stéphane Lathuilière. Towards image compression with perfect realism at ultra-low bitrates. In *The Twelfth International Conference on Learning Representations*, 2023.
- [11] Zhengxue Cheng, Heming Sun, Masaru Takeuchi, and Jiro Katto. Learned image compression with discretized gaussian mixture likelihoods and attention modules. In *Proceedings of the IEEE/CVF conference on computer vision and pattern recognition*, pages 7939–7948, 2020.
- [12] Yoojin Choi, Mostafa El-Khamy, and Jungwon Lee. Variable rate deep image compression with a conditional autoencoder. In *Proceedings of the IEEE/CVF international conference on computer vision*, pages 3146–3154, 2019.
- [13] Eastman Kodak Company. Kodak lossless true color image suite. <http://r0k.us/graphics/kodak/>, 1993. Original images, commonly used as a test set for image compression.
- [14] Keyan Ding, Kede Ma, Shiqi Wang, and Eero P Simoncelli. Image quality assessment: Unifying structure and texture similarity. *IEEE transactions on pattern analysis and machine intelligence*, 44(5):2567–2581, 2020.
- [15] Patrick Esser, Robin Rombach, and Bjorn Ommer. Taming transformers for high-resolution image synthesis. In *Proceedings of the IEEE/CVF conference on computer vision and pattern recognition*, pages 12873–12883, 2021.
- [16] Runsen Feng, Zongyu Guo, Weiping Li, and Zhibo Chen. Nvtc: Nonlinear vector transform coding. In *Proceedings of the IEEE/CVF Conference on Computer Vision and Pattern Recognition*, pages 6101–6110, 2023.
- [17] Ge Gao, Pei You, Rong Pan, Shunyuan Han, Yuanyuan Zhang, Yuchao Dai, and Hojae Lee. Neural image compression via attentional multi-scale back projection and frequency decomposition. In *Proceedings of the IEEE/CVF International Conference on Computer Vision*, pages 14677–14686, 2021.
- [18] Dailan He, Ziming Yang, Weikun Peng, Rui Ma, Hongwei Qin, and Yan Wang. Elic: Efficient learned image compression with unevenly grouped space-channel contextual adaptive coding. In *Proceedings of the IEEE/CVF conference on computer vision and pattern recognition*, pages 5718–5727, 2022.
- [19] Dailan He, Yaoyan Zheng, Baocheng Sun, Yan Wang, and Hongwei Qin. Checkerboard context model for efficient learned image compression. In *Proceedings of the IEEE/CVF Conference on Computer Vision and Pattern Recognition*, pages 14771–14780, 2021.

- [20] Martin Heusel, Hubert Ramsauer, Thomas Unterthiner, Bernhard Nessler, and Sepp Hochreiter. Gans trained by a two time-scale update rule converge to a local nash equilibrium. *Advances in neural information processing systems*, 30, 2017.
- [21] Seungmin Jeon, Kwang Pyo Choi, Youngo Park, and Chang-Su Kim. Context-based trit-plane coding for progressive image compression. In *Proceedings of the IEEE/CVF Conference on Computer Vision and Pattern Recognition*, pages 14348–14357, 2023.
- [22] Zhaoyang Jia, Jiahao Li, Bin Li, Houqiang Li, and Yan Lu. Generative latent coding for ultra-low bitrate image compression. In *Proceedings of the IEEE/CVF Conference on Computer Vision and Pattern Recognition*, pages 26088–26098, 2024.
- [23] Wei Jiang, Jiayu Yang, Yongqi Zhai, Peirong Ning, Feng Gao, and Ronggang Wang. Mlic: Multi-reference entropy model for learned image compression. In *Proceedings of the 31st ACM International Conference on Multimedia*, pages 7618–7627, 2023.
- [24] Nick Johnston, Damien Vincent, David Minnen, Michele Covell, Saurabh Singh, Troy Chinen, Sung Jin Hwang, Joel Shor, and George Toderici. Improved lossy image compression with priming and spatially adaptive bit rates for recurrent networks. In *Proceedings of the IEEE conference on computer vision and pattern recognition*, pages 4385–4393, 2018.
- [25] Jun-Hyuk Kim, Byeongho Heo, and Jong-Seok Lee. Joint global and local hierarchical priors for learned image compression. In *Proceedings of the IEEE/CVF Conference on Computer Vision and Pattern Recognition*, pages 5992–6001, 2022.
- [26] Ivan Krasin, Tom Duerig, Neil Alldrin, Vittorio Ferrari, Sami Abu-El-Haija, Alina Kuznetsova, Hassan Rom, Jasper Uijlings, Stefan Popov, Andreas Veit, et al. Openimages: A public dataset for large-scale multi-label and multi-class image classification. *Dataset available from <https://github.com/openimages>*, 2(3):18, 2017.
- [27] Jooyoung Lee, Seunghyun Cho, and Seung-Kwon Beack. Context-adaptive entropy model for end-to-end optimized image compression. *arXiv preprint arXiv:1809.10452*, 2018.
- [28] Jooyoung Lee, Seyoon Jeong, and Munchul Kim. Selective compression learning of latent representations for variable-rate image compression. *Advances in Neural Information Processing Systems*, 35:13146–13157, 2022.
- [29] Eric Lei, Hamed Hassani, and Shirin Saeedi Bidokhti. Approaching rate-distortion limits in neural compression with lattice transform coding. *arXiv preprint arXiv:2403.07320*, 2024.
- [30] Anqi Li, Feng Li, Yuxi Liu, Runmin Cong, Yao Zhao, and Huihui Bai. Once-for-all: Controllable generative image compression with dynamic granularity adaption. *arXiv preprint arXiv:2406.00758*, 2024.
- [31] Meng Li, Shangyin Gao, Yihui Feng, Yibo Shi, and Jing Wang. Content-oriented learned image compression. In *European Conference on Computer Vision*, pages 632–647. Springer, 2022.
- [32] Mu Li, Wangmeng Zuo, Shuhang Gu, Debin Zhao, and David Zhang. Learning convolutional networks for content-weighted image compression. In *Proceedings of the IEEE conference on computer vision and pattern recognition*, pages 3214–3223, 2018.
- [33] Chaoyi Lin, Jiabao Yao, Fangdong Chen, and Li Wang. A spatial rnn codec for end-to-end image compression. In *Proceedings of the IEEE/CVF Conference on Computer Vision and Pattern Recognition*, pages 13269–13277, 2020.
- [34] Jinming Liu, Heming Sun, and Jiro Katto. Learned image compression with mixed transformer-cnn architectures. In *Proceedings of the IEEE/CVF conference on computer vision and pattern recognition*, pages 14388–14397, 2023.
- [35] Fabian Mentzer, Eirikur Agustsson, Michael Tschanen, Radu Timofte, and Luc Van Gool. Conditional probability models for deep image compression. In *Proceedings of the IEEE conference on computer vision and pattern recognition*, pages 4394–4402, 2018.
- [36] Fabian Mentzer, George D Toderici, Michael Tschanen, and Eirikur Agustsson. High-fidelity generative image compression. *Advances in neural information processing systems*, 33:11913–11924, 2020.
- [37] David Minnen, Johannes Ballé, and George D Toderici. Joint autoregressive and hierarchical priors for learned image compression. *Advances in neural information processing systems*, 31, 2018.
- [38] David Minnen and Saurabh Singh. Channel-wise autoregressive entropy models for learned image compression. In *2020 IEEE International Conference on Image Processing (ICIP)*, pages 3339–3343. IEEE, 2020.
- [39] Anish Mittal, Rajiv Soundararajan, and Alan C Bovik. Making a “completely blind” image quality analyzer. *IEEE Signal processing letters*, 20(3):209–212, 2012.
- [40] Guanbo Pan, Guo Lu, Zhihao Hu, and Dong Xu. Content adaptive latents and decoder for neural image compression. In *European Conference on Computer Vision*, pages 556–573. Springer, 2022.
- [41] Oren Rippel and Lubomir Bourdev. Real-time adaptive image compression. In *International conference on machine learning*, pages 2922–2930. PMLR, 2017.
- [42] Claude E Shannon et al. Coding theorems for a discrete source with a fidelity criterion. *IRE Nat. Conv. Rec*, 4(142-163):1, 1959.
- [43] Chajin Shin, Hyeongmin Lee, Hanbin Son, Sangjin Lee, Dogyoon Lee, and Sangyoun Lee. Expanded adaptive scaling normalization for end to end image compression. In *European Conference on Computer Vision*, pages 390–405. Springer, 2022.

- [44] George Toderici, Lucas Theis, Nick Johnston, Eirikur Agustsson, Fabian Mentzer, Johannes Ballé, Wenzhe Shi, and Radu Timofte. Clic 2020: Challenge on learned image compression. *Retrieved March, 29:2021*, 2020.
- [45] Guo-Hua Wang, Jiahao Li, Bin Li, and Yan Lu. Evc: Towards real-time neural image compression with mask decay. *arXiv preprint arXiv:2302.05071*, 2023.
- [46] Fei Yang, Luis Herranz, Yongmei Cheng, and Mikhail G Mozerov. Slimmable compressive autoencoders for practical neural image compression. In *Proceedings of the IEEE/CVF Conference on Computer Vision and Pattern Recognition*, pages 4998–5007, 2021.
- [47] Ruihan Yang and Stephan Mandt. Lossy image compression with conditional diffusion models. *Advances in Neural Information Processing Systems*, 36:64971–64995, 2023.
- [48] Richard Zhang, Phillip Isola, Alexei A Efros, Eli Shechtman, and Oliver Wang. The unreasonable effectiveness of deep features as a perceptual metric. In *Proceedings of the IEEE conference on computer vision and pattern recognition*, pages 586–595, 2018.
- [49] Xi Zhang and Xiaolin Wu. Attention-guided image compression by deep reconstruction of compressive sensed saliency skeleton. In *Proceedings of the IEEE/CVF Conference on Computer Vision and Pattern Recognition*, pages 13354–13364, 2021.
- [50] Xi Zhang and Xiaolin Wu. Multi-modality deep restoration of extremely compressed face videos. *IEEE Transactions on Pattern Analysis and Machine Intelligence*, 45(2):2024–2037, 2022.
- [51] Xi Zhang and Xiaolin Wu. Lvqac: Lattice vector quantization coupled with spatially adaptive companding for efficient learned image compression. In *Proceedings of the IEEE/CVF Conference on Computer Vision and Pattern Recognition*, pages 10239–10248, 2023.
- [52] Xi Zhang and Xiaolin Wu. Learning optimal lattice vector quantizers for end-to-end neural image compression. *Advances in Neural Information Processing Systems*, 37:106497–106518, 2024.
- [53] Xiaosu Zhu, Jingkuan Song, Lianli Gao, Feng Zheng, and Heng Tao Shen. Unified multivariate gaussian mixture for efficient neural image compression. In *Proceedings of the IEEE/CVF Conference on Computer Vision and Pattern Recognition*, pages 17612–17621, 2022.
- [54] Yin hao Zhu, Yang Yang, and Taco Cohen. Transformer-based transform coding. In *International conference on learning representations*, 2022.